Enhancement of photoluminescence from silicon nanocrystals by metal nanostructures made by nanosphere lithography

Yugo Mochizuki,[1] Minoru Fujii,[1,a)] Shinji Hayashi,[1] Takaaki Tsuruoka,[2] and Kensuke Akamatsu[2]
[1]*Department of Electrical and Electronic Engineering, Graduate School of Engineering, Kobe University, Rokkodai, Nada, Kobe 657-8501, Japan*
[2]*Frontiers of Innovative Research in Science and Technology, Konan University, Minatojima-minamimachi, Chuo-ku, Kobe 650-0047, Japan*

(Received 26 March 2009; accepted 1 June 2009; published online 9 July 2009)

The effect of metal nanostructures prepared by nanosphere lithography on photoluminescence (PL) properties of silicon nanocrystals (Si-ncs) is studied. By placing Ag nanotriangles or Au nanovoids on SiO_2 films containing Si-ncs, the PL intensity is enhanced. For the sample having Ag nanotriangles, the largest PL enhancement is obtained when the excitation wavelength coincides with the absorption band of Ag nanotriangles. This suggests that the enhancement of the incident field by surface plasmon polariton (SPP) excitation is responsible for the PL enhancement. On the other hand, for the sample having Au nanovoids, the PL enhancement is mainly made by the enhancement of effective radiative decay rate of Si-ncs by efficient excitation and scattering of SPPs. © *2009 American Institute of Physics*. [DOI: 10.1063/1.3159030]

I. INTRODUCTION

A Si-based light emitting device is one of the most important optical elements in realizing Si-based optoelectronic circuits that integrate electronic and photonic elements on a Si wafer. Silicon nanocrystals (Si-ncs) have been attracting great interests as a key material of Si-based light emitting devices. Si-ncs exhibit visible and near infrared luminescence at room temperature due to the recombination of quantum confined excitons.[1–4] Confinement of excitons in a space smaller than the exciton Bohr radius of bulk Si crystals increases the overlap of electron and hole wave functions in both real and momentum spaces, resulting in the enhancement of the radiative recombination rate.[2,3] However, even for Si-ncs as small as a few nanometers in diameter, indirect band gap nature of bulk Si crystals is strongly inherited,[5] and thus the spontaneous emission rate is still not large enough compared to that of direct band gap semiconductor and the luminescence quantum efficiency is rather low.[2,3] Therefore, the improvement of the luminescence property is very important for their application to light emitting devices.

One of the approaches to enhance luminescence of Si-ncs is to utilize the coupling of electronic excitation of Si-ncs to surface plasmon polaritons (SPPs) supported by metal nanostructures. For example, by placing a nanoporous gold (Au) layer near Si-ncs, enhancement of the photoluminescence (PL) intensity was demonstrated.[6–10] The SPP resonance energy can be controlled in a wide wavelength range by the size and the shape of metal nanostructures. By placing a silver (Ag) island array with different sizes and pitches near Si-ncs, PL enhancement at specific wavelength ranges was achieved.[6] The PL enhancement was also observed for a simple system consisting of a flat metal film and an organic grating.[7,8] Metal films with rough surface are also reported to exhibit strong PL enhancement.[10] The enhancement is usually explained by electromagnetic coupling of excitons in Si-ncs with dipolar plasmon modes of metal nanostructures.[9,11]

From previous studies on SPP mediated PL enhancement of Si-ncs, it has been recognized that the precise control of the shape and arrangement of metal nanostructures is essential in obtaining desirable PL properties. In previous studies, the metal structures were mainly produced by electron-beam lithography.[12] Although high-resolution precise patterns can be achieved by the electron-beam lithography, the technique is time consuming and not cost effective. Nanosphere lithography (NSL) is a simple and low cost process to fabricate various kinds of periodic nanostructures. In this technique, the submicron latex spheres self-assembled into a hexagonal pattern are used as a template to create various kinds of ordered two-dimensional (2D) array of desired materials. Its effectiveness for the formation of metal nanostructures has been demonstrated.[13] For example, Ag nanotriangles and Au nanovoids have possibility of stronger PL enhancement than simple structures made by conventional lithography technique due to their abrasive shapes.

The purpose of this work is to demonstrate the effectiveness of the NSL technique for the PL enhancement of Si nanocrystals. We study PL properties of Si-ncs having metal nanostructures made by NSL. We prepare two types of metal nanostructures, i.e., a Ag nanotriangle array and a Au nanovoid array, and study how PL properties of Si-ncs are modified by the metal nanostructures. We also discuss the mechanism of PL enhancement from PL excitation spectra, angle, and polarization resolved PL spectra and PL time transients.

II. SAMPLE PREPARATION

SiO_2 films containing Si-ncs (Si-nc:SiO_2) were prepared by a cosputtering method.[14,15] Si and SiO_2 were simulta-

a)Electronic mail: fujii@eedept.kobe-u.ac.jp.

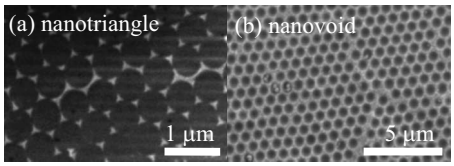

FIG. 1. SEM images of a Ag nanotriangle array and a Au nanovoid array.

neously sputter deposited on a SiO_2 substrate and the deposited films (150 nm in thickness) were annealed in a nitrogen gas atmosphere for 30 min at 1150 °C. To prepare a Ag nanotriangle array, Ag was deposited by vacuum evaporation through a 2D crystal of polystyrene (PS) nanospheres placed on the Si-nc:SiO_2 films.[13] The diameter of PS nanospheres was 500 nm. The height of Ag nanotriangles was controlled by the thickness of Ag. After the Ag deposition, the PS nanosphere templates were removed by immersing the samples in toluene for several hours. For the preparation of a Au nanovoid array, a Ti film (5 nm in thickness) and a Au film (20 nm in thickness) were deposited on Si-nc:SiO_2 films prior to the formation of 2D crystal of PS nanospheres (750 nm in diameter). Through the PS nanosphere crystal Au was grown by an electrochemical plating. The thickness of Au was controlled by monitoring the current during the plating. PS nanospheres were removed by toluene after the Au growth. Figures 1(a) and 1(b) show scanning electron microscope (SEM) images of the surface of the sample with a Ag nanotriangle array and a Au nanovoid array, respectively.

III. RESULTS AND DISCUSSION

A. Ag nanotriangle array

Figures 2(a) and 2(b) show transmittance (T) and reflectance (R) spectra, respectively, for the samples with different

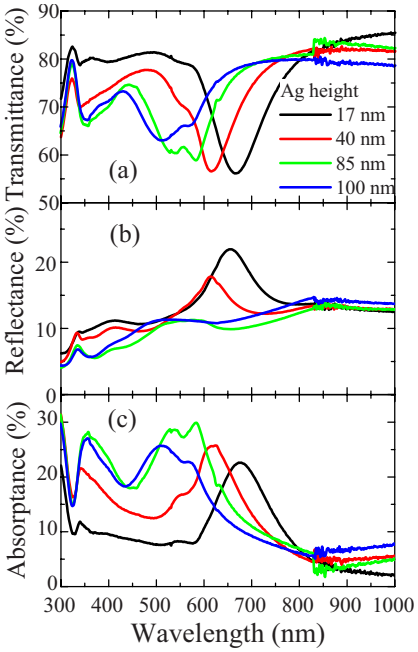

FIG. 2. (Color online) (a) Transmittance, (b) reflectance, and (c) absorptance spectra of the samples with Ag nanotriangle arrays. The height of Ag nanotriangles is changed from 17 to 100 nm.

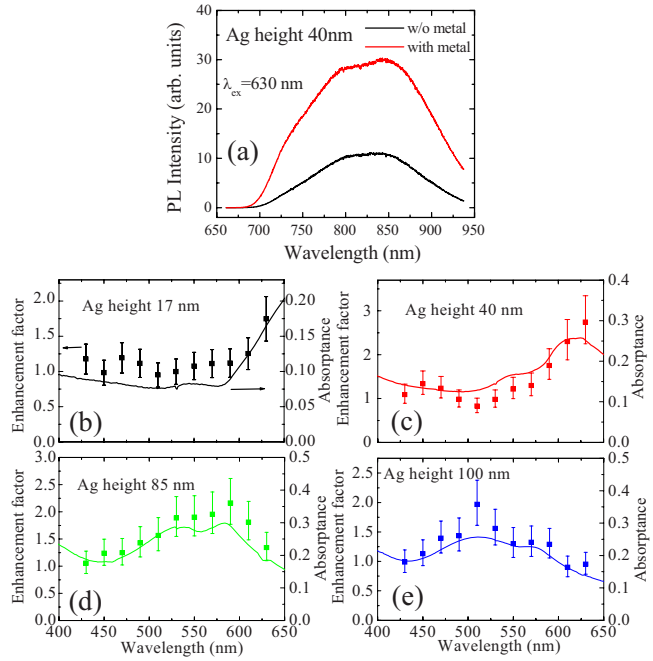

FIG. 3. (Color online) (a) PL spectra of the sample with and without a Ag nanotriangle array. The height of Ag nanotriangles is 40 nm. Excitation wavelength is 630 nm. [(b)–(e)] Absorptance spectra (solid curves) (right axis) and excitation wavelength dependence of PL enhancement factors (filled squares) (left axis). The error bars represent maximum and minimum values. Ag nanotriangle heights are (b) 17, (c) 40, (d) 85, and (e) 100 nm, respectively.

height Ag nanotriangles. The incident angle of the reflectance measurement is 5°. Figure 2(c) shows the absorptance (A) defined by 1-T-R. The absorptance corresponds to the number of photons absorbed by the sample. In Fig. 2(c), two bands are seen around 350 and 500–700 nm. The 350 nm band is assigned to the interband transition of Ag, while the 500–700 nm band is due to the excitation of localized SPPs. The SPP band shifts toward shorter wavelength with increasing the Ag nanotriangle height. The shift is mainly due to the change in the aspect ratio with increasing the height.[16,17]

Figure 3(a) compares PL spectra of Si-ncs with and without Ag nanotriangles. The excitation source for the PL measurements is the optical parametric oscillator pumped by the third harmonic of a Nd:YAG laser (pulse width of 5 nm, repetition of 20 Hz). The excitation wavelength is 630 nm. The samples are excited from the substrate side with the incident angle of 45° and detected from the same side by using a single grating monochromator with a liquid nitrogen cooled charge coupled device. The solid angle of the PL detection is about 18°. The spectral response of the detection system is corrected with the aid of a reference spectrum of a standard tungsten lamp. In Fig. 3(a), a broad PL band due to the recombination of excitons in Si-ncs is seen around 800 nm in both samples. PL intensity is enhanced by a factor of 3 by the Ag nanotriangles. In Figs. 3(b)–3(e), the PL enhancement factors are plotted as a function of the excitation wavelength for the samples with the Ag heights of 17, 40, 85, and 100 nm, respectively. The PL enhancement factors are obtained by dividing PL spectra of the sample with metal by that without metal. The excitation wavelength is changed from 430 to 630 nm. The absorptance spectra are also shown

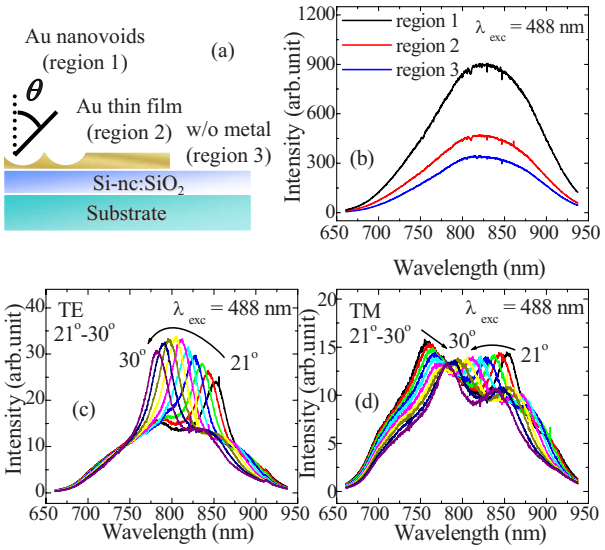

FIG. 4. (Color online) (a) Schematic illustration of sample structure, (b) PL spectra of regions 1, 2, and 3. Excitation wavelength is 488 nm. [(c) and (d)] Angle and polarization dependence of PL spectra of region 1. The detection angle is changed from 21° to 30°. (c) TE polarization and (d) TM polarization.

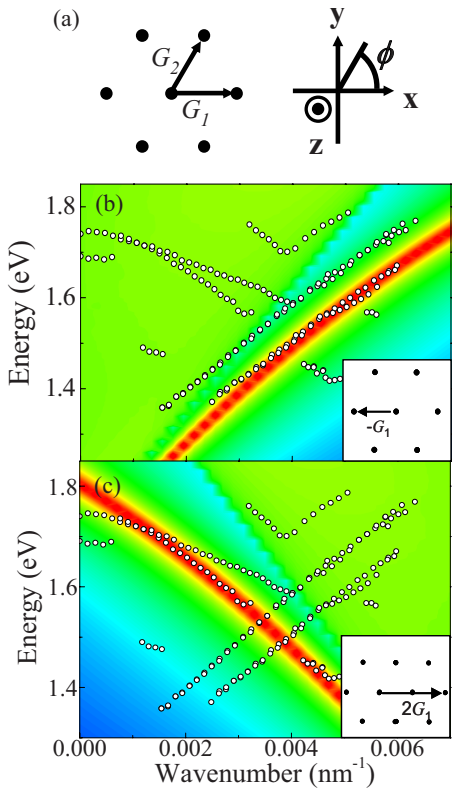

FIG. 5. (Color online) (a) Definition of grating vectors and coordinates. [(b) and (c)] Dispersion relations. Circles correspond to experimentally obtained data. The color map is obtained by calculation. The region in red color represents larger power dissipation. The scattering orders (m,n) are (b) $(-1,0)$ and (c) (2,0). The insets are corresponding grating vectors.

in the same figures. The excitation wavelength dependence of the PL enhancement factors coincides very well with that of the absorptance spectra. This is a clear evidence that PL is enhanced by strong fields accompanies by the excitation of localized SPPs of Ag nanotriangles. Figure 3 also demonstrates that the wavelength of the largest PL enhancement can be controlled simply by changing the height of Ag nanotriangles.

B. Au nanovoid array

Figure 4(a) shows a schematic illustration of the sample with a Au nanovoid array. We prepare three regions in each sample to make exact comparison of the PL intensity possible. Region 1 has Au nanovoids, while region 2 has a Au thin flat film. Region 3 is a bear sample without metal. Figure 4(b) shows the PL spectra for regions 1, 2, and 3. The excitation source is a 488 nm line of an Ar ion laser. The excitation light is incident from the substrate side with the angle of 45° and the PL is detected from the same side of the sample. The solid angle of the PL detection is about 18°. The PL intensity of region 2 is enhanced by a factor of 1.5 compared to that of region 3. This is simply due to the reflection of incident and emitted light by the Au thin film. In region 1, the PL intensity is enhanced by a factor of 2.7 compared to that of region 3 and by a factor of 2.0 compared to that of region 2.

The PL from region 1 has strong angle dependence. For the measurement of the angle dependence of PL spectra, the excitation light is illuminated normal to the surface through the transparent fused quartz substrate and the PL is detected from the sample surface, i.e., from the side of Au nanovoids, by changing the angle θ from 0° (normal to the surface) to 50° [Fig. 4(a)]. PL was detected through an aperture approximately 1 mm in diameter, which limits the angular acceptance to about 1°. Figures 4(c) and 4(d) show the angle dependent PL spectra for TE and TM polarizations, respectively. TE and TM polarizations are defined as their electric fields being perpendicular and parallel to the incident plane, respectively. The PL peak wavelength shifts depending on the detection angle in both the TE and TM polarizations. From the angle dependence of PL peak wavelengths, the dispersion relations are obtained. The experimentally obtained dispersion relations are shown in Fig. 5 by open circles. To facilitate the comparison with calculation, the same experimental data are displayed in both Figs. 5(b) and 5(c).

In order to assign the modes, we calculate the dispersion relations by the formula developed by Chance *et al.*,[18] by assuming a four-layer system consisting of air/Au/Si-nc:SiO_2/SiO_2. In the calculation, an emitter is regarded as an oscillating electric dipole and the power dissipated from an isotropic dipole positioned at the center of a Si-nc:SiO_2 layer is calculated as a function of a wavenumber. For the calculation, the refractive indices of Au, Si, and SiO_2 are taken from literature[19–22] and that of the Si-nc:SiO_2 layer is estimated from the Bruggeman effective medium theory.[23] In the presence of a grating, the wave vector of SPP is augmented or reduced. Figure 5(a) shows the definition of the grating vectors ($\vec{G}_1$ and $\vec{G}_2$) and coordinates. For a 2D grating, the coupling condition between radiative modes propagating in the x-z plane and nonradiative modes, such as SPPs, propagating in the x-y plane is expressed as

$$k_m(\omega)\begin{pmatrix}\cos\phi\\ \sin\phi\end{pmatrix}+m\mathbf{G}\begin{pmatrix}1\\0\end{pmatrix}+n\mathbf{G}\begin{pmatrix}1/2\\ \sqrt{3}/2\end{pmatrix}=\begin{pmatrix}k_{\parallel}(\omega)\\0\end{pmatrix}$$
$$=\begin{pmatrix}k_0(\omega)\sin\theta\\0\end{pmatrix}, \quad (1)$$

where $k_m(\omega)$ and $k_{\parallel}(\omega)$ denote the in-plane wave vector of the mode and the emitted light, respectively, $k_0(\omega)$ represents the absolute value of the wave vector of the emitted light, ω is the angular frequency, ϕ is the azimuthal angle of the propagation of nonradiative modes, θ is the polar angle of the propagation of radiative modes, $\mathbf{G}=|\vec{G}_1|=|\vec{G}_2|=2\pi/\Lambda$ is the grating vector with the grating period Λ, and m and n are the orders of the scattering process arising from the grating vectors $\vec{G}_1$ and $\vec{G}_2$, respectively. In order to reproduce experimentally obtained dispersion relations, we adjusted the values of the grating period. The best result is obtained when the grating period is 800 nm. This value is slightly different from the actual diameter of PS nanospheres. Similar deviation of the effective grating period from the actual PS nanosphere diameter has been reported by some groups[13,24] and is considered to arise from the deviation of the metal nanostructure shape from the sine wave. At the wavelength range of Si-ncs emission, SPPs experience two scattering processes, i.e., $(m,n)=(-1,0),(2,0)$.

The calculated dispersion relations are shown in Figs. 5(b) and 5(c) by color gradients. The insets are the corresponding grating vectors. The red region and the blue one represent larger and smaller power dissipations, respectively. The strong power dissipation corresponds to the SPP modes propagating at the interface between Au and the active layer (Au/Si-nc:SiO_2 SPP). In Figs. 5(b) and 5(c), the overall agreement between calculated and experimentally obtained dispersion relation is good. The agreement indicates that the emission from region 1 mainly arises from the coupling of excitons in Si-ncs to SPPs. In Figs. 5(b) and 5(c), small difference is seen between the calculated and experimentally obtained dispersion relations. This probably arises from small deviation of actual refractive index of the active layer from that estimated from the Bruggeman effective medium theory and from too simplified assumption in the calculation that the metal film is flat. Furthermore, in Fig. 5, modes that are not identified by calculation exist. They may arise from the scattering by defects in the periodic structure.

The inset of Fig. 6(a) shows the PL decay curves for regions 1, 2, and 3 detected at 830 nm. For time-resolved PL measurements, the samples were excited by a 405 nm laser diode. The signals were detected by a near infrared photomultiplier tube (R5509-72, Hamamatsu Photonics). The time resolution of the system was about 3 μs. The decay rates of the samples with a Au nanovoid array (region 1) and a Au thin film (region 2) are larger than that of the region without Au (region 3). The larger decay rates in regions 1 and 2 are due to dissipation of the excitation energy to Au nanovoids and Au thin films, respectively. No significant difference of the decay rates can be seen in regions 1 and 2, indicating that the existence of nanovoids structure does not influence the decay rate. In order to investigate the wavelength dependence of the decay rates, we measure PL decay curves in the

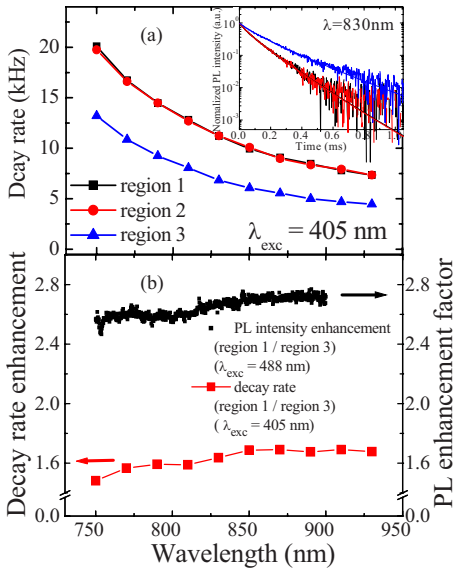

FIG. 6. (Color online) (a) Wavelength dependence of PL decay rates for regions 1 (filled square), 2 (filled circle), and 3 (filled triangle). Inset: PL decay curves of regions 1, 2, and 3 detected at 830 nm. Decay curves of regions 1 and 2 are very similar. (b) The wavelength dependence of PL intensity enhancement factor (right axis) and decay rate enhancement factor (left axis).

750–930 nm region and estimated the decay rates by fitting the decay curves by a stretched exponential function.[25] The results are shown in Fig. 6(a). Closed squares, circles, and triangles represent PL decay rates obtained from regions 1, 2, and 3, respectively. In all cases, the decay rate increases at shorter wavelengths, i.e., when PL from smaller Si-ncs is detected. This is due to the increase in the radiative decay rate by the quantum size effect.[26] The decay rate of regions 1 and 2 are always larger than that of region 3 in the whole emission wavelength range.

Figure 6(b) shows the enhancement factors of the decay rate obtained by dividing the decay rate of region 1 by that of region 3 (left axis). On the right axis, the enhancement factors of the PL intensity are also shown. The enhancement factors of the decay rate and the intensity show very similar wavelength dependence. This indicates that the PL enhancement is mainly due to the enhancement of the effective radiative decay rate by efficient excitation and scattering of SPPs supported by Au nanovoids. Note that, in the case of Au nanovoids, PL enhancement due to the enhanced incident field is not expected because the excitation wavelengths (488 or 405 nm) are far from the SPP resonance wavelength.

IV. CONCLUSION

We demonstrated the effectiveness of metal nanostructures made by NSL for the improvement of PL properties of Si-ncs. By placing Ag nanotriangles and Au nanovoids on top of SiO_2 films containing Si-ncs, enhancements of the PL intensity by factors of 3 and 2.7 were achieved. For the sample having Ag nanotriangles, the largest PL enhancement was obtained when the excitation wavelength coincides with the absorption band of Ag nanotriangles. This suggests that the enhancement of the incident field by SPP excitation is responsible for the PL enhancement. On the other hand, for

the sample having Au nanovoids, the enhancement was mainly made by the enhancement of the effective radiative decay rate of Si-ncs by efficient excitation and scattering of SPPs. Within the present work, either the excitation efficiency or the radiative decay rate was enhanced depending on the shape and the kinds of metal. By refining the design of the metal structure, e.g., by combining the two structures in this work, simultaneous enhancement of the both processes may be possible.

ACKNOWLEDGMENTS

This work was supported by a Grant-in-Aid for Scientific Research from the Ministry of Education, Culture, Sports, Science and Technology, Japan.

[1]L. T. Canham, Appl. Phys. Lett. **57**, 1046 (1990).
[2]C. Delerue, M. Lannoo, G. Allan, and E. Martin, Thin Solid Films **255**, 27 (1995).
[3]D. Kovalev, H. Heckler, G. Polisski, and F. Koch, Phys. Status Solidi B **215**, 871 (1999).
[4]S. Takeoka, M. Fujii, and S. Hayashi, Phys. Rev. B **62**, 16820 (2000).
[5]I. Sychugov, R. Juhasz, J. Valenta, and J. Linnros, Phys. Rev. Lett. **94**, 087405 (2005).
[6]J. S. Biteen, N. Lewis, H. A. Atwater, H. Mertens, and A. Polman, Appl. Phys. Lett. **88**, 131109 (2006).
[7]E. Takeda, T. Nakamura, M. Fujii, S. Miura, and S. Hayashi, Appl. Phys. Lett. **89**, 101907 (2006).
[8]E. Takeda, M. Fujii, T. Nakamura, Y. Mochizuki, and S. Hayashi, J. Appl. Phys. **102**, 023506 (2007).
[9]H. Mertens, J. S. Biteen, H. A. Atwater, and A. Polman, Nano Lett. **6**, 2622 (2006).
[10]K. Okamoto, A. Scherer, and Y. Kawakami, Phys. Status Solidi **5**, 2822 (2008) (c).
[11]H. Mertens and A. Polman, J. Appl. Phys. **105**, 044302 (2009).
[12]J. S. Biteen, D. Pacifici, N. S. Lewis, and H. A. Atwater, Nano Lett. **5**, 1768 (2005).
[13]R. M. Cole, Y. Sugawara, J. J. Baumberg, S. Mahajan, M. Abdelsalam, and P. N. Bartlett, Phys. Rev. Lett. **97**, 137401 (2006).
[14]Y. Kanzawa, T. Kageyama, S. Takeoka, M. Fujii, S. Hayashi, and K. Yamamoto, Solid State Commun. **102**, 533 (1997).
[15]M. Fujii, A. Mimura, S. Hayashi, and K. Yamamoto, Appl. Phys. Lett. **75**, 184 (1999).
[16]K. L. Shuford, M. A. Ratner, and G. C. Schatz, J. Chem. Phys. **123**, 114713 (2005).
[17]W. Huang, W. Qian, and M. A. El-Sayed, J. Phys. Chem. B **109**, 18881 (2005).
[18]R. R. Chance, A. Prock, and R. Silbey, Adv. Chem. Phys. **37**, 1 (1978).
[19]W. L. Barnes, J. Mod. Opt. **45**, 661 (1998).
[20]D. W. Lynch and W. R. Hunter, *Handbook of Optical Constants of Solids*, edited by E. D. Palik (Academic, Orlando, FL, 1985).
[21]D. F. Edwards, *Handbook of Optical Constants of Solids*, edited by E. D. Palik (Academic, Orlando, FL, 1985).
[22]H. R. Philipp, *Handbook of Optical Constants of Solids*, edited by E. D. Palik (Academic, Orlando, FL, 1985).
[23]P. A. Snow, E. K. Squire, P. S. J. Russell, and L. T. Canham, J. Appl. Phys. **86**, 1781 (1999).
[24]T. A. Kelf, Y. Sugawara, R. M. Cole, J. J. Baumberg, M. E. Abdelsalam, S. Cintra, S. Mahajan, A. E. Russell, and P. N. Bartlett, Phys. Rev. B **74**, 245415 (2006).
[25]G. Mauckner, K. Thonke, T. Baier, T. Walter, and R. Sauer, J. Appl. Phys. **75**, 4167 (1994).
[26]S. Miura, T. Nakamura, M. Fujii, M. Inui, and S. Hayashi, Phys. Rev. B **73**, 245333 (2006).